Convolutional Neural Networks for Classifying the Stages of the Cell Cycle

Duque-Vazquez Edgar F.[1,1], Cepeda-Negrete Jonathan[2,2†], López-Meza Joel E.[3,3†], Saldana-Robles Noe[4,1†], Sanchez-Yanez Raul E.[1,1*†]

[1]Department of Agricultural Engineering, Universidad de Guanajuato, Ex Hacienda El Copal km 9; carretera Irapuato-Silao; A.P. 311, Irapuato, 36500, Guanajuato, Mexico.

[2*]Department of Electronic Engineering, Universidad de Guanajuato, Carretera Salamanca - Valle de Santiago km 3.5 + 1.8 Comunidad de Palo Blanco, Salamanca, 36885, Guanajuato, Mexico.

[3]Centro Multidisciplinario de Estudios en Biotecnología de la facultad de Medicina Veterinaria y Zootecnia, Universidad Michoacana de San Nicolas de Hidalgo, Km 9.5 Carretera Morelia-Zinapécuaro, Posta Veterinaria, Morelia, 58893, Michoacan, México.

*Corresponding author(s). E-mail(s): sanchezy@ugto.mx;
Contributing authors: ef.duquevazquez@ugto.mx; j.cepeda@ugto.mx; elmeza@umich.mx; saldanar@ugto.mx;
†These authors contributed equally to this work.

Abstract

The cell cycle represents a highly coordinated process, and any potential dysregulation may lead to cellular anomalies with carcinogenic risk, emphasizing the critical importance of its observation. To address this necessity, tasks such as classification have been proposed, employing both biological techniques such as FUCCI and computational approaches involving deep learning models. However, current tools exhibit an inherent propensity for errors. In this context, our study focuses on methodological improvement through the development of a convolutional neural network model designed to achieve a more precise classification of cell cycle states. Throughout this investigation, we constructed and evaluated a convolutional neural network model using an imbalanced dataset. In this process, we drew upon methodologies proposed by other researchers, incorporating

data augmentation techniques. The evaluation of our model revealed a remarkable classification capability for cell cycle phases, achieving a weighted average of 93.72% using the F1 metric. This model not only proved to be more congruent with the type of data employed but also achieved a more accurate classification of cell cycle states. This outcome underscores the distinctive ability of a convolutional neural network to classify patterns in the cell cycle more accurately than human perception, which, by its nature, can be prone to errors.

Keywords: jurkat, machine learning, imbalanced, cancer

1 Introduction

The cell cycle is a highly coordinated process that encompasses two general states: interphase and mitosis. Each of these states is divided into specific phases. The interphase is subdivided into three phases: G1, S, and G2, in that order. Mitosis, on the other hand, is divided into four phases: prophase, metaphase, anaphase, and telophase [1].

In the study of a cell, the analysis of the cell cycle is of great significance. Inadequate regulation of the cell cycle can lead to cell abnormalities, which, in turn, may contribute to the development of diseases such as cancer [2]. These abnormalities can be prevented and diagnosed through the observation and analysis of each of the cell cycle states.

Alterations in cell morphology during the various phases of the cell cycle are typically minimal from a visual standpoint. In this context, we provide a brief explanation of what occurs in each of the phases, as well as the extent of the changes observed in cell morphology thereafter.

The G1 phase is the first phase of the cell cycle, where the cell synthesizes proteins and RNA. In this phase, the cell doesn't show significant morphological differences. In the S phase, the cell initiates with subtle morphological changes that may not be discernible to the naked eye. These changes are a result of DNA synthesis. In the G2 phase, the cell begins to duplicate its organelles, leading to a significant morphological change compared to the other two phases of the cycle. In prophase and metaphase, cells do not exhibit morphological differences visible to the human eye. However, this changes in anaphase, where the cell begins to elongate in preparation for division. When the cell reaches telophase, it is almost completely divided, making the visual morphological change evident.

The observation of cell alterations is carried out through microscopy techniques. The most commonly used methods in cell cycle analysis range from the use of flow cytometry [3] to the calculation of DNA content in the cell [4]. Biomarkers such as FUCCI technology [5] are also utilized. However, it is important to note that the mentioned techniques do not provide extensive details about cell morphology in each phase of the cell cycle [6].

In world, data analysis is permeating virtually every field of research. Cell cycle analysis is no exception, as the use of computer vision or machine learning techniques enables the classification of cell cycle phases using images. This task, which is challenging to perform with the naked eye, is still being performed manually.

The use of deep learning networks is the most commonly employed tool when it comes to cell cycle phase classification. Abin et al. utilized a Recurrent Neural Network in combination with Convolutional Gated Recurrent Unit layers in two of their works for cell cycle classification. In both studies, a comparison was made with a ResNet [7] [8].

Narotamo et al. uses FUCCI technology as an indicator to determine the cell cycle phase. In their work, they emphasize the use of the DAPI compound, which is employed for identifying the cell nucleus, particularly in cell cycle studies. In their cell cycle analysis studies, they employed a Support Vector Machine (SVM) for phase classification [5]. Additionally, in another study, they proposed three approaches based on the Fast YOLO algorithm and the use of the DAPI compound for cell staining, primarily for classifying phases corresponding to the cell cycle interphase [9]. On another note, Rappez et al. created a deep neural network called DeepCycle to reconstruct the cell cycle trajectory. In this approach, as in previous works, they employed FUCCI technology [10].

Our study is part of a broader context and is closely related to several previous works due to the dataset we use. We will now present these works based on their chronology, which will allow us to contextualize our approach and highlight the current contributions in the field.

Eulenberg et al. reconstructed the cell cycle with the aim of demonstrating its behavior in the progression of diabetic retinopathy. They implemented a neural network based on MXNet, which they named DeepFlow, for classifying the different cell cycle states, achieving an accuracy of 79.40% when considering the seven cell cycle states. In some phases, the algorithm's classification turns out to be deficient due to the limited quantity of images [11]. In response to the clear limitations of the Eulenberg et al. algorithm, new research emerged, which introduced alternative approaches to tackle the issue.

Jin et al. introduced the use of the WGAN-GP data augmentation technique to mitigate the issue of data imbalance, particularly in the phases of cell division. Subsequently, they implemented a ResNet-41 model. Considering the classification of the seven phases, they reported an accuracy of 82.10% [6].

Rana et al. presented two studies in which they classified the cell cycle. Similar to Jin et al., they addressed the issue of data imbalance by employing a combination of two data augmentation techniques: WGAN and "mixup." In their results, they achieved an accuracy of 85% [12]. In their second study, they combined three data augmentation techniques: WGAN, "mixup" and nonlinear "mixup," resulting in an accuracy of 85.6% [13].

Despite the use of data augmentation techniques in each of the articles presented, the issue of low classification results in each of the cell cycle phases, especially during mitosis, still persists. In this work, we introduce an algorithm capable of classifying the phases of the cell cycle with higher accuracy than the algorithms mentioned.

The article is divided into four sections following this introduction. In the next section, we will present the methodology used. Subsequently, the results will be introduced through images and graphs, along with their discussion. Finally, we will present the conclusions reached at the end of this study.

2 Results

The presented work introduces a CNN model designed to classify the different phases of a cancerous cell cycle. This model was trained using images from the Jurkat cell line. To validate the efficiency of the developed model, a comprehensive comparison was conducted between the obtained results and those of other deep learning models utilizing the same database, as detailed in the introduction and methodology of the work. The selected metrics for model evaluation include precision, recall, the F1 score, and the weighted average of the F1 score. It is crucial to note that, during the evaluation of the proposed model, a 5-fold stratified cross-validation was employed. In this section, the evaluation and discussion are divided into two parts: the first regarding the dataset without modifications, the second concerning the data set with data augmentation using the WGAN-GP and WGAN-div + mixup techniques.

Evaluation of CNN model with out used modifications

In this study, the adoption of a Convolutional Neural Network (CNN) was based on several considerations. The utilization of a CNN is characterized by reduced complexity and heightened suitability, primarily owing to the available volume of data, which aligns seamlessly with the requisites of a moderately deep network. Furthermore, the deployment of a CNN is associated with reduced computational overhead and faster data processing.

The magnitude and heterogeneity of the training dataset constitute pivotal determinants for the efficacy of the developed model. In particular, for classes G1, S and G2, a substantial volume of data facilitates the facile assimilation of common patterns by the model. However, the remarkable resemblance observed among images from distinct classes presents a challenge to the model's classification accuracy, particularly concerning class S. This intricacy is discernible in the confusion matrix illustrated in Figure 1, in which the model exhibits a propensity to classify class S with classes G1 and G2, thereby contributing to a reduction in overall model accuracy.

Conversely, classes associated with mitosis feature a severely restricted number of images within both the training and validation sets. The model's task becomes increasingly arduous as it struggles to adequately discern specific patterns within these classes.

Due to the inherent characteristics of the utilized data, encompassing the quantity per class and the overall size of the data set, the network tends to exhibit overfitting tendencies toward classes with larger samples. Consequently, this phenomenon engenders suboptimal performance, exerting a direct influence on the overarching efficacy of the model. The termination of model training at epoch 22 was prompted by discernible shifts in the loss function of the validation data.

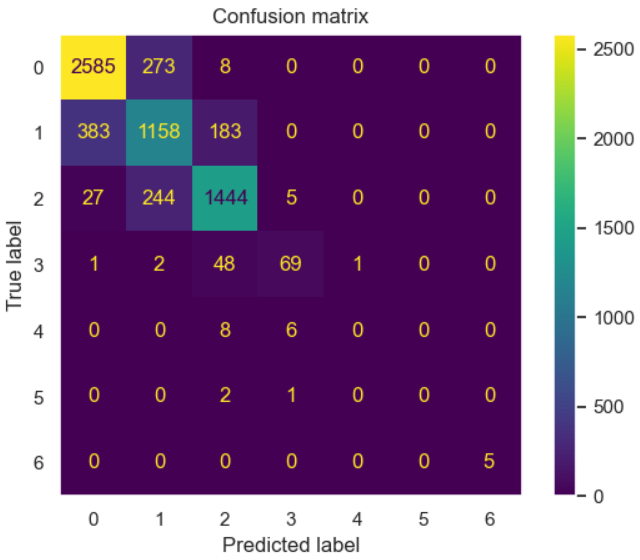

Fig. 1 Confusion matrix of the classification of the dataset without modifications.

In order to assess the performance of the proposed model, a comparison was made with the data published by Jin et al. (see Table 1). In said table, it is evident that the imbalance in the quantity of data per class emerges as an influential factor in the model's performance. Positive outcomes are highlighted for the G1, G2 and Telophase phases, largely attributable to the abundance of data and the clarity of the object to be classified in the images, in contrast to other phases. The metric values obtained reveal a significant difference that favors our model in comparison to that of Jin et al.

Table 1 Class-wise comparison of the unaltered dataset between the proposed model and Jin et al.

Phase	Precision		Recall		F1	
Model	Jin et al.	Proposal	Jin et al.	Proposal	Jin et al.	Proposal
G1	0.8316	0.8628	0.8403	0.9020	0.8359	0.8820
S	0.6765	0.6905	0.7052	0.6717	0.6905	0.6810
G2	0.8453	0.8529	0.8012	0.8395	0.8241	0.8462
Prophase	0.8521	0.8519	1.0000	0.5702	0.9202	0.6832
Metaphase	0.0000	0.0000	0.0000	0.0000	0.0000	0.0000
Anaphase	0.0000	0.0000	0.0000	0.0000	0.0000	0.0000
Telophase	0.0000	1.0000	0.0000	1.0000	0.0000	1.0000
Weighted Average	0.7835	0.8117	0.7844	0.8152	0.7853	0.8127

2.1 Results of the CNN architecture trained with data augmentation techniques

To address the data imbalance, Jin et al. proposed the implementation of the WGAN-GP data augmentation technique, coupled with undersampling in the G1 phase. The methodology of by Jin et al. was adopted to assess the performance of the proposed CNN model, now incorporating data augmentation techniques.

Figure 2 displays the confusion matrix of the model trained with data augmentation and G1 undersampling. Recalling the challenges encountered with imbalanced data, an increase in the number of true positives in class S is observed, while the count of true negatives and false negatives has slightly decreased. Furthermore, in states associated with mitosis, a notable increase in true positives is evident, a result of incorporating new data provided by the data augmentation technique.

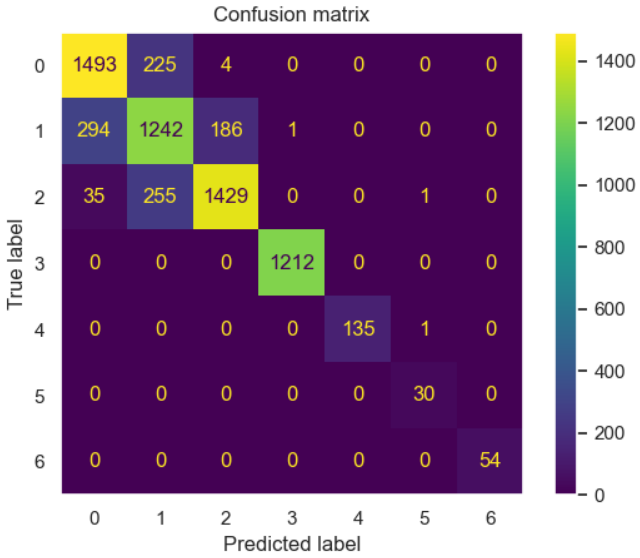

Fig. 2 Confusion matrix of the classification of the dataset using the WGAN-GP data augmentation technique.

Table 2 showcases improvements in most phases in terms of metrics, unlike the imbalanced dataset, for both the methodology proposed by Jin et al. and the proposed CNN model. The results of our model, in particular, are superior, suggesting that the utilization of a conventional CNN model can yield classification results similar to or even better than other deep learning architectures.

Rana et al. conducted a study in which they trained a ResNet using images generated by combining the data augmentation techniques WGAN-div + mixup. We have relied on their proposed methodology, adapting it to the proposed CNN model. The proposed CNN was trained, and a superior performance was observed per epoch for

Table 2 Class-wise comparison between the proposed model and Jin et al. using the dataset with WGAN-GP data augmentation and oversampling in the G1 stage.

Phase	Precision		Recall		F1	
Model	Jin et al.	Proposal	Jin et al.	Proposal	Jin et al.	Proposal
G1	0.8181	0.8194	0.8490	0.8670	0.8333	0.8426
S	0.6700	0.7213	0.6918	0.7208	0.6808	0.7210
G2	0.8456	0.8826	0.7895	0.8308	0.8166	0.8559
Prophase	0.9934	0.9992	0.9909	1.0000	0.9922	0.9996
Metaphase	0.8125	1.0000	0.9559	0.9926	0.8784	0.9963
Anaphase	1.0000	0.9375	0.0667	1.0000	0.1250	0.9677
Telophase	1.0000	1.0000	1.0000	1.0000	1.0000	1.0000
Weighted Average	0.8210	0.8490	0.8184	0.8481	0.8174	0.8481

both the training and validation data compared to the process undertaken by Jin et al. and the data without the use of data augmentation techniques.

In the confusion matrix shown in the Figure 3, one can appreciate the low number of false positives and false negatives. Focusing specifically on the classes related to mitosis, an almost perfect classification is observed, achieved through the use of data augmentation techniques. It is important to note that, visually, the states of mitosis may appear different from each other, making differentiation more evident through the use of more examples.

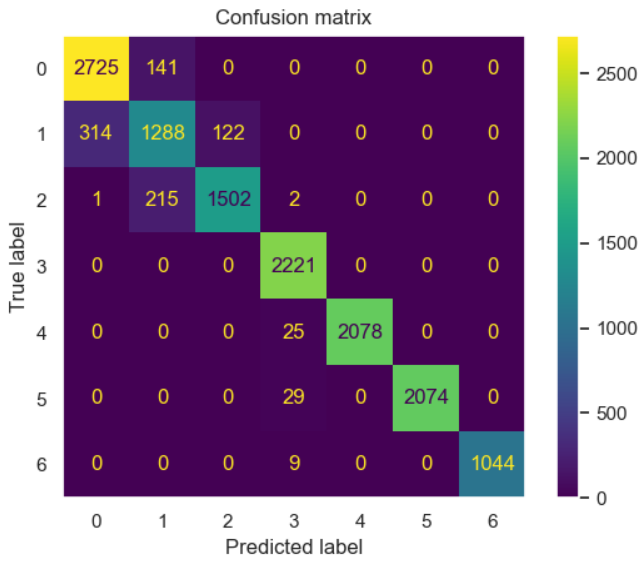

Fig. 3 Confusion matrix of the classification of the dataset using the WGAN-div and mixup data augmentation techniques.

In general, we can affirm that the developed model, fueled by examples provided by a WGAN-div, demonstrated superior performance. In the Table 3, a comparison with the methodology proposed by Rana et al. is observed, focusing specifically on the F1 metric, where the algorithm shows good results in the majority of cell cycle states. With this, we can confirm that the proposed model enhances its efficiency by incorporating additional data.

Table 3 Class-wise comparison between the proposed model and Rana et al. using the dataset with WGAN-div data augmentation and *mixup*.

Phase	Rana et al.	Proposal
G1	0.9300	0.9280
S	0.7500	0.7648
G2	0.8400	0.8983
Prophase	0.9200	0.9856
Metaphase	0.5700	0.9940
Anaphase	1.0000	0.9931
Telophase	1.0000	0.9951
Weighted Average	0.8600	0.9372

3 Methodology

In this section, the methodology employed in the development of the proposed CNN model in this work is detailed. Initially, the details of the dataset used are presented. Subsequently, the intricacies of the architecture of the developed CNN model are described. Finally, a brief explanation is provided regarding the methodologies of the methods with which we conducted comparisons, along with a description of the functioning of the metrics used to assess the performance of the developed model.

3.1 Dataset

The dataset used was extracted from the work of Eulenberg et al citeeulenberg2017reconstructing. This dataset comprises four channels (brightfield, darkfield, and fluorescence channels), each with 32,266 images. These images correspond to cancer cells from the Jurkat cell line and were captured through imaging flow cytometry.

In this study, the brightfield and darkfield channels were used. The dataset is divided into seven classes (states), corresponding to the phases of the cell cycle: G1, S, G2 (interphase), and Profase, Metafase, Anafase, and Telofase (mitosis). The distribution of images per class is presented in Figure 4. The images have a size of 66x66 pixels and are in color format.

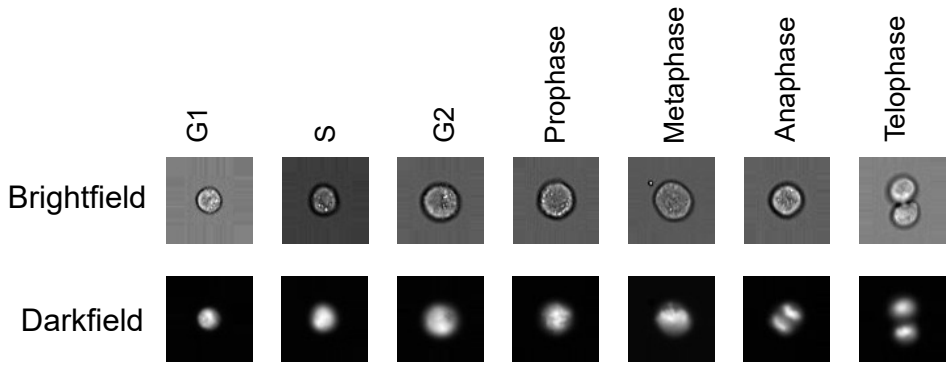

Fig. 4 Images of the cell cycle arranged by phase, employed in this study.

3.2 Developed CNN model

Given the specific characteristics of the data, a Convolutional Neural Network (CNN) model has been designed, following standard conventions in the field. This model consists of two convolutional layers, each followed by a max-pooling layer. The convolutional layers are configured with kernels of 64 and 32, which learn the features of the image. The kernel sizes are 10 and 5, respectively. The activation function used in each of these layers is Rectified Linear Unit (ReLU).

Subsequently, the flattening technique was implemented and connected to a dense layer composed of 32 neurons, followed by a dropout layer to mitigate the risk of overfitting. Then, another dense layer with 16 neurons was used; in both dense layers, the ReLU activation function was applied. Finally, a dense layer with 7 neurons was incorporated, each representing one of the cell cycle states to be classified. Consequently, a softmax activation function was applied to the last layer, facilitating the classification of the different categories (see Figure 5).

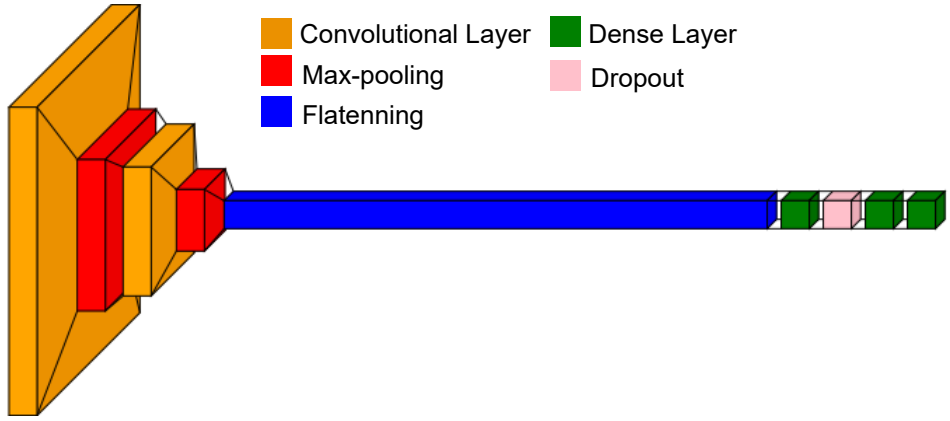

Fig. 5 Built Convolutional Neural Network Architecture

3.3 Train model

The network was trained with the dataset mentioned in the methodology, which was split into two sets: training data (80% of the images) and test data (20% of the images). The model was compiled using a categorical cross-entropy loss function, commonly employed in multiclass classification problems. The Adam optimization function was used with a learning rate of 0.0001, $beta_1$=0.9, and $beta_2$=0.999, along with a batch size of 32. Finally, accuracy was employed as a metric to assess the model's performance during both training and evaluation.

The dataset used exhibited data imbalance in the phases corresponding to mitosis, posing a potential overfitting problem during training. To address this, the authors who utilized the same dataset chose to employ data augmentation techniques to achieve a balance in the amount of data per class. The data augmentation techniques used were WGAN-GP [14] and WGAN-div [15] in combination with *mixup* [16]. These techniques are explained in detail below.

3.4 Development of other methodologies

Based on the methodology of Jin et al., the data augmentation technique WGAN-GP was employed. The network was trained using a batch size of 4 for Anafase and Telofase, and 16 for Metafase and Profase. Training was carried out for 7000 epochs, with a learning rate of 0.00001, $beta_1 = 0.01$ and $beta_2 = 0.999$. The size of the images was adjusted from $66 \times 66 \times 3$ to $64 \times 64 \times 3$. The network hyperparameters were kept at their default values. This was done to achieve a balance between the mitosis classes and the interphase classes. However, the G1 class had an excess of samples, so undersampling was applied by randomly removing images from the G1 phase.

With the new data set ready, the model developed in section 3.2 was trained with the initially assigned hyperparameters, obtaining new performance values for the classification of cell cycle states.

Similarly, based on the methodology of Rana et al., the data augmentation technique WGAN-div was used in combination with the *mixup* technique. The batch size for all classes was 64, while the learning rate was 0.0001 for Profase, Metafase and Anafase, and 0.00001 for Telofase, $beta_1 = 0.01$ and $beta_2 = 0.999$. Like WGAN-GP, the size of the images was adjusted from $66 \times 66 \times 3$ to $64 \times 64 \times 3$. The number of training steps for the discriminator per iteration was 10 for Profase and 4 for Metafase, Anafase and Telofase. The network hyperparameters were kept at their default values. Half of the images obtained by WGAN-GP had the *mixup* technique applied and were combined with the images obtained by WGAN and the original images. With this new dataset, the model developed in Section 3.2 of this chapter was trained with the hyperparameters initially assigned.

3.5 F1-Score

The F1-score metric is commonly employed in the evaluation of classification models, as it combines two key metrics: precision and recall. The standard practice involves using these metrics together to provide a comprehensive assessment of the model's

performance. F1 reaches its optimal value at 1 and its minimum at 0 [17]. The F1 score is calculated using the Formula 1.

$$F1 = \frac{2 \cdot (Precision \cdot Recall)}{(Precision + Recall)} \tag{1}$$

where F1 is given by 2 and 3

$$Precision = \frac{TruePositives}{TruePositives + FalsePositives} \tag{2}$$

$$Recall = \frac{TruePositives}{TruePositives + FalseNegatives} \tag{3}$$

4 Conclusion

This project successfully achieved the classification of the 7 states in the cycle of a cancerous cell. It was demonstrated that a standard CNN model is capable of effectively classifying the phases of the cell cycle even in an imbalanced dataset. The efficiency of the CNN model is enhanced by applying data augmentation techniques. Phases of the cell cycle, which may be challenging for the human eye to observe, can be accurately classified using a deep learning model. Additionally, data augmentation techniques prove invaluable when a dataset lacks a sufficient number of images per class. This approach allows for a more robust training of the model, resulting in improved performance when assessing the model's accuracy with diverse data.

Acknowledgments. Edgar F. Duque-Vazquez thanks the Mexican National Council on Humanities, Sciences and Technology (CONAHCYT) for the scholarship grant 1081409.

Declarations

References

[1] Caglar, H.O., Biray Avci, C.: Alterations of cell cycle genes in cancer: unmasking the role of cancer stem cells. Molecular biology reports **47**, 3065–3076 (2020)

[2] Coffman, J.A.: Cell cycle development. Developmental cell **6**(3), 321–327 (2004)

[3] FANG, H.-S., LANG, M.-F., SUN, J.: New methods for cell cycle analysis. Chinese Journal of Analytical Chemistry **47**(9), 1293–1301 (2019) https://doi.org/10.1016/S1872-2040(19)61186-2

[4] Roukos, V., Pegoraro, G., Voss, T.C., Misteli, T.: Cell cycle staging of individual cells by fluorescence microscopy. Nature protocols **10**(2), 334–348 (2015)

[5] Narotamo, H., Fernandes, M.S., Moreira, A.M., Melo, S., Seruca, R., Silveira, M., Sanches, J.M.: A machine learning approach for single cell interphase cell cycle staging. Scientific Reports **11**(1), 19278 (2021)

[6] Jin, X., Zou, Y., Huang, Z.: An imbalanced image classification method for the cell cycle phase. Information **12**(6), 249 (2021)

[7] Jose, A., Roy, R..i.-.e.j., Stegmaier, J.: Weakly-supervised temporal segmentation of cell-cycle stages with center-cell focus using recurrent neural networks. In: BVM Workshop, pp. 212–219 (2023). Springer

[8] Jose, A., Roy, R., Eschweiler, D., Laube, I., Azad, R., Moreno-Andrés, D., Stegmaier, J.: End-to-end classification of cell-cycle stages with center-cell focus tracker using recurrent neural networks. In: ICASSP 2023-2023 IEEE International Conference on Acoustics, Speech and Signal Processing (ICASSP), pp. 1–5 (2023). IEEE

[9] Narotamo, H., Fernandes, M.S., Sanches, J.M., Silveira, M.: Interphase cell cycle staging using deep learning. In: 2020 42nd Annual International Conference of the IEEE Engineering in Medicine & Biology Society (EMBC), pp. 1432–1435 (2020). IEEE

[10] Rappez, L., Rakhlin, A., Rigopoulos, A., Nikolenko, S., Alexandrov, T.: Deepcycle reconstructs a cyclic cell cycle trajectory from unsegmented cell images using convolutional neural networks. Molecular systems biology **16**(10), 9474 (2020)

[11] Eulenberg, P., Köhler, N., Blasi, T., Filby, A., Carpenter, A.E., Rees, P., Theis, F.J., Wolf, F.A.: Reconstructing cell cycle and disease progression using deep learning. Nature communications **8**(1), 463 (2017)

[12] Rana, P., Sowmya, A., Meijering, E., Song, Y.: Imbalanced cell-cycle classification using wgan-div and mixup. In: 2022 IEEE 19th International Symposium on Biomedical Imaging (ISBI), pp. 1–4 (2022). IEEE

[13] Rana, P., Sowmya, A., Meijering, E., Song, Y.: Data augmentation for imbalanced blood cell image classification. bioRxiv, 2022–08 (2022)

[14] Gulrajani, I., Ahmed, F., Arjovsky, M., Dumoulin, V., Courville, A.C.: Improved training of wasserstein gans. Advances in neural information processing systems **30** (2017)

[15] Wu, J., Huang, Z., Thoma, J., Acharya, D., Van Gool, L.: Wasserstein divergence for gans. In: Proceedings of the European Conference on Computer Vision (ECCV), pp. 653–668 (2018)

[16] Zhang, H., Cisse, M., Dauphin, Y.N., Lopez-Paz, D.: mixup: Beyond empirical risk minimization. arXiv preprint arXiv:1710.09412 (2017)

[17] Rijsbergen, C.: Information retrieval 2nd ed buttersworth. London, 115 (1979)